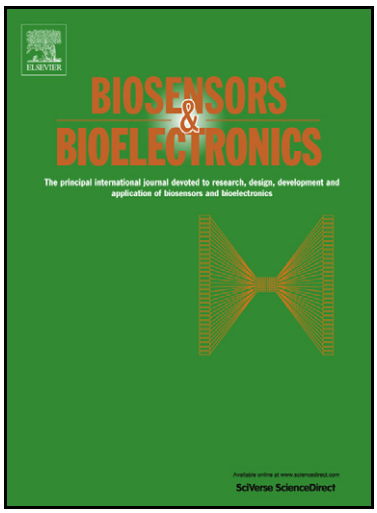

www.elsevier.com/locate/bios

Detection of DNA hybridization by field-effect DNA-based biosensors: Mechanisms of signal generation and open questions

A.G. Cherstvy

PII: S0956-5663(13)00124-3
DOI: http://dx.doi.org/10.1016/j.bios.2013.02.026
Reference: BIOS5768

To appear in: *Biosensors and Bioelectronics*

Received date: 8 January 2013
Revised date: 5 February 2013
Accepted date: 13 February 2013

Cite this article as: A.G. Cherstvy, Detection of DNA hybridization by field-effect DNA-based biosensors: Mechanisms of signal generation and open questions, *Biosensors and Bioelectronics,* http://dx.doi.org/10.1016/j.bios.2013.02.026

Detection of DNA hybridization by field-effect DNA-based biosensors: mechanisms of signal generation and open questions

A. G. Cherstvy [1,*]

[(1)] *Institute for Physics and Astronomy, University of Potsdam, 14476 Potsdam-Golm, Germany*

* email: a.cherstvy@gmail.com

Phone: +49-3319775953

Abstract

We model electrostatic effects taking place upon DNA hybridization in dense DNA arrays immobilized on a layer of Au nano-particles deposited on the surface of a field-effect-based DNA capacitive biosensor. We consider the influence of separation of a charged analyte form the sensor surface and the salinity of electrolyte solution, in the framework of both linear and nonlinear Poisson-Boltzmann theories. The latter predicts a substantially weaker sensor signals due to electrostatic saturation effects. We analyze how different physical parameters of dense DNA probe brushes affect the magnitude of hybridization signals. The list includes the fraction of DNA charge neutralization, the length and spatial conformations of adsorbed DNA molecules, as well as the discreteness of DNA charges. We also examine the effect of Donnan ionic equilibrium in DNA lattices on the sensor response. The validity of theoretical models is contrasted against recent experimental observations on detection of DNA hybridization via its intrinsic electric charge. The sensitivity of such biochemical sensing devices, their detection limit, and DNA hybridization efficiency are briefly discussed in the end.

Abbreviations: FED field-effect device, EISOI electrolyte-insulator-semiconductor silicon-on-insulator structure, GNP gold nano-particle, ss single-stranded, ds double-stranded, bp base pair, ES electrostatic, PB Poisson-Boltzmann, [salt] salt concentration.

Key Words: DNA hybridization, Au nano-particle, bio-electrochemical sensing, electrostatic screening.

1. Introduction

1.1 Detection of charged macromolecules

A number of methods with different signal-to-noise ratio and applicability range have extensively been used for detection of nucleic acids fragments from aqueous mixtures. Among them are optical (fluorescence correlation spectroscopy [1], fluorescence resonance energy transfer [2]) and spectroscopic (surface enhanced Raman scattering [3]) methods, mechanical micro-cantilever setups [4,5,6,7], surface plasmon resonance [8], electro-hydro-dynamical devices [9], some nano-wires [10,11] and carbon nanotubes apparatus [12], as well as various semiconductor-based biosensors [13,14,15,16,17,18]. Many optical methods involve labeling of probe molecules that is time-consuming and often costly, while some other devices

implement DNA amplification by polymerase chain reaction method that is not very sequence-specific [19,20,21]. Electro-chemical techniques that use DNA biosensors functionalized with conducting nano-rods [22], carbon nanotubes [23,24,25,26,27], and lipid-DNA hybrids [28] have also been developed and characterized. Basic concepts and recent developments in the DNA field-effect device (FED) bio-sensing were reported in Refs. [29,30].

DNA detection limit of biosensors is often in nM-pM range in [DNA]; some ultra-sensitive devices with detectable [DNA]~10 fM were also reported recently [31]. The selectivity of the devices is often a single mismatch in the DNA nucleotide sequence for the probe and target DNA molecules [32,33]. Many methods above are focused on DNA nucleotide polymorphism imperative for a number of genomic and medical applications, while the other can be used to detect the level of DNA methylation important for epigenetic DNA analysis.

Label-free direct detection of charged bio-macro-molecules using FED biosensors provides a fast, sensitive and low-cost method to detect DNA sequences (as well as proteins and enzymes) at low concentrations from unknown solutions. Chemical modifications and functionalizations of the silicone surface for label-free DNA detection found numerous applications in biomedicine, genetics, food and drug industry. This method allows to avoid a number of obstacles of molecular labeling methods and offers a new approach for a next-generation DNA chips with direct electrical readout for parallel low-cost high-throughput DNA sequence analysis.

The focus of this theoretical study is DNA hybridization on the surface of DNA biosensor. It is a straightforward tool to bring the charges of complementary DNA sequences from solution to the sensor surface. The mechanism of signal generation is then the intrinsic DNA charge [34]. The primary obstacle of electrostatic (ES) DNA detection via its intrinsic charge is a screening of DNA charges by mobile ions in electrolyte. This could significantly reduce the expected sensor signal, especially at high ionic strengths when the Debye screening length λ_D is short (e.g., $\lambda_D \approx 1$ nm in 0.1 M of 1:1 salt). The FEDs can only detect the potential changes that occur within 1-2 λ_D from the sensor surface. A number of experimental [35], theoretical [36,37,38] and computer simulation [39,40] studies appeared recently on the effect of intrinsic macromolecular charge and screening in application to DNA biosensors.

1.2. Experimental Setup: Au-nano-particle-DNA hybrids

The procedure of fabrication of a novel lab-on-a-chip nano-plate electrolyte-insulator-semiconductor silicon-on-insulator (EISOI) biosensor array functionalized with gold nano-particles (GNPs) for detection [41,42,43] of DNA hybridization has been described in details in our recent paper [44] as well as in Ref. [45]. Shortly, GNPs were strongly covalently bound onto a silanized sensor surface. Likewise, thiol-modified probe 20 base pair (bp) long single-stranded (ss) DNA sequences were immobilized onto GNPs, see FIG. 1. The GNP sensor-surface coverage evaluated from SEM images was 60-70% [45]. This results in GNP surface density of $\rho_{GNP} \approx (1\text{-}1.3)\times 10^{16}$ GNPs/m^2 for an average GNP-particle diameter of D~50-80 Å. The sensor response was characterized by the constant capacitance method [35], which enables a direct monitoring of potential changes caused by DNA hybridization at the gate-electrolyte interface. The hybridization was shown to be very efficient for fully-matched sequences of probe and target ss-DNAs, while no hybridization took place for the fully-mismatched ss-DNA fragments [45]. It remains to be understood how sensitive such a sensor performs for partially-matched DNA sequences (work in progress).

A positive signal shift in the constant capacitance mode corresponds to a more negative gate surface charge. This can be attributed to an additional negative charge of hybridized (double stranded) ds DNA (see Ref. [45] for more details on measurement protocols and the mechanisms of signal generation). The observed hybridization signals were unexpectedly large, $\Delta\varphi \approx$90-120 mV [45,46], that is 3-4 times higher than the signals reported with a capacitive EIS sensor without modification by GNP-DNA hybrids, $\Delta\varphi \approx$24-33 mV [47,48]. This potential change $\Delta\varphi$ is the reduction of the ES potential measured on the sensor interface upon the hybridization of probe ss-DNAs on the lattice with complementary target ss-DNAs from the solution. In experiments, the DNA hybridization has been performed at high salinities of the solution (0.1 M PBS, 0.9 M NaCl) to ease the formation of DNA duplex between probe and target DNA single strands. DNA charges are strongly screened at high salt and can thus hybridize easier. To maximize the hybridization signal, the readout to the sensor response was done on the contrary at very low salinities (0.2 mM PBS).

GNP-GNA hybrids present an electro-chemical bio-recognition element that transduces the target-DNA-signal to the sensor surface. GNPs not only provide ES coupling of DNA charge with the sensor gate, they also ensure a substantial signal amplification, similar to an amplified pH-sensitivity in polyelectrolyte multilayer structures on FEDs [49]. The layer of deposited GNPs likely allows a more regular and denser deposition of probe ss-DNAs. The spherical/convex GNP shape effectively increases the electrode surface area available for DNA adsorption and thereby yields overall higher DNA densities per unit sensor surface [50]. A finite diameter of GNPs as well as an extended nature of the immobilized probe ss-DNA molecules requires a more detailed evaluation of DNA ES effects. This is the main purpose of this study, as compared to a number of models available in the literature, where the DNA charges were modelled as adsorbed right on the sensor surface.

1.3. DNA charge parameters

The ds-DNA is a highly-charged helical polyelectrolyte with the radius of a=9 Å and helical pitch of 34 Å. It bares 2 negative phosphate charges every base pair that results in the linear charge density of one elementary charge $-e_0$ per l_0=1.7 Å along the DNA axis. The major part of this charge is neutralized by adsorbed counterions from the solution ($\theta_{ds}\approx 0.75$ in mono-valent salts, according to the Manning theory [51,52]), while the rest is screened in a diffuse layer by mobile ions. The cations are attracted to DNA to ensure its electro-neutrality and to reduce the ES self-energy [53,54]. The ss-DNA is much more flexible than ds-DNA (≈30 vs. ≈500 Å persistence length l_p) [55], it has about half the radius and half the linear charge density of ds-DNA. The phosphate-phosphate separation along the helix of a ds-DNA is ≈7 Å.

Due to a loose 3D structure and inter-charge distance comparable to the Bjerrum length, l_B, ss-DNA charge neutralization fraction θ_{ss} is not very well-defined. Based on the axial charge density, the fraction θ_{ss} should be smaller than $\theta_{ds} \approx 1-l_0/l_B$. Note that in both our previous studies on detection of DNA intrinsic charges [57,44], we assumed $\theta_{ss}=\theta_{ds}$ that effectively doubles the charge density of ss-DNA brush upon DNA hybridization. We analyze this aspect in more details below. The fraction θ_{ds} measurably depend on [salt] in solution and it grows in the presence of 2- and 3-valent cations in the buffer.

1.4. Linear vs. nonlinear PB models

The linear Poisson-Boltzmann (PB) model is the standard tool to estimate the magnitude of ES effects in changed systems, including dense DNA assemblies [56] and DNA brushes [57]. It works particularly well for salinities close to and above the biological one that is $n_0\approx 0.1$ M of NaCl that corresponds to $\lambda_D\approx 10$ Å. This length defines a typical length-scale of the decay of ES potential from a point charge, as well as from charged planar and curved interfaces [58]. Coulomb long-range ES forces are rendered effectively short-range by this screening. For low salinities, $n_0\approx 0.001$-0.01 M, the linear PB theory becomes non-applicable and it can strongly overestimate the potential magnitude, $|\varphi|$. The limit here is φ=25 mV or the dimensionless ES potential of

EQ. 1 $$\Psi = e_0\varphi/(k_BT) = 1 .$$

Here k_BT is the thermal energy or the energy of interaction of two e_0 charges at separation

EQ. 2

$$l_B = e_0^{\,2}/(\varepsilon k_BT)$$

in water (here $\varepsilon\approx 80$ is the water dielectric constant). Often, for DNA the linear PB theory works quite well for potentials up to 25-50 mV. To save space here, we address the reader to Refs. [59,60] where the applicability regimes of the linear PB theory have been analyzed in terms of the screening length, surface charge density, and surface geometry. The non-linear PB theory works for arbitrary high ES potentials in the mean-field limit, but it enables the analytical solution only in some simple geometries and with special boundary conditions.

1.5. Physical principles of sensor signal generation

The rate and efficiency of DNA hybridization depends in particular on the ionic strength in solution (faster at higher [salt]), DNA concentration (typically faster at higher [DNA]), ambient temperature (ds-DNA formation is more efficient at lower T), DNA length (shorter sequences hybridize typically faster), as well as the density of DNA lattice (see the Discussion). To minimize the ES screening of DNA charges and to achieve higher sensor signals, DNA hybridization has been performed in Ref. [44] at a high ionic strength (0.9 M NaCl). The changes in the output sensor signal due to DNA hybridization were readout on the contrary in a low ionic strength (0.2 mM PBS at pH 7.5, see the details in Ref. [45]). Other ways to improve DNA hybridization efficiency might involve application of a positive voltage to the sensor surface to attract the target ss-DNAs from solution more efficiently [61].

The effect of DNA brush density is here three-fold. Higher densities of the probe ss-DNAs yield larger final electric charges in the vicinity of the sensor surface. In contrast, very dense DNA lattices impede penetration of target ss-DNA strands into the DNA brush and inhibit complementarity recognition with the probe ss-DNAs. Also, an effective Donnan-Debye screening length in dense DNA lattices [56] is shorter due to a progressive accumulation of mobile ions, see Sec. 2.1.3. below.

The length of immobilized DNA probes also plays a dual role. Longer DNAs yield higher overall charges, but the hybridization kinetics and efficiency will be inhibited. This poses inherent limitations to the length of DNAs that can be detected by the method proposed in Ref. [44]. In that study, the DNAs were 20 bp long that ensures a fast hybridization (minutes) and reproducible sensor signals. Also, for longer DNA fragments the effect of terminal DNA phosphates (the charges far from the sensor surface) will be screened stronger resulting in a non-monotonic signal with the DNA length, see Sec. 2.1.1.

One more aspect is due to DNA chain flexibility and DNA conformational changes upon hybridization. Namely, the layer of ss-DNA is rather floppy, while the brush of hybridized ds-DNAs is comparably stiff. This effectively "pushes away" the charges of ds-DNAs from the sensor surface, particularly for longer DNA fragments with L>>30 Å, likely reducing the magnitude of the final signal $\Delta\varphi$ detected due to DNA hybridization.

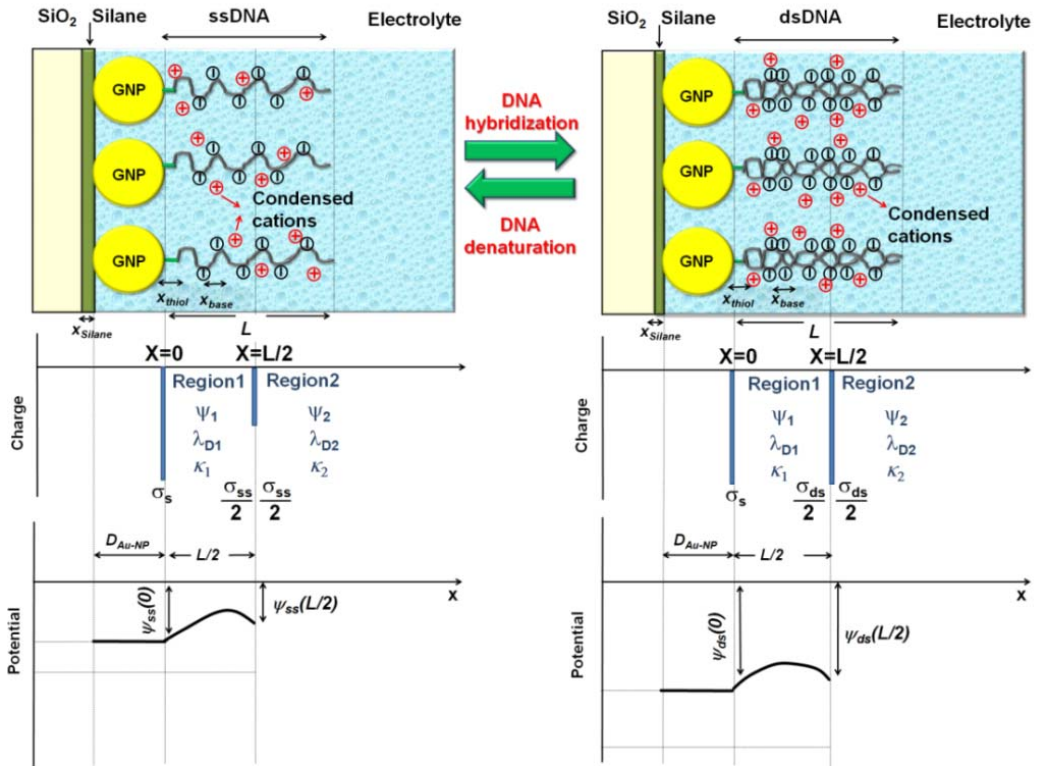

FIG. 1. Schematics of SiO_2 surface functionalized with GNP-DNA hybrids and the changes in the sensor potential upon DNA hybridization and denaturation. Both ss-and ds-DNAs are oriented normal to the sensor surface. The magnitudes of the charge densities on the sensor surface (σ_s) and on the ss- and ds-DNA sheets in the DNA middle (σ_{ss} and σ_{ds}) are also shown as the blue bars. As GNPs are good conductors, in the model the value of the ES potential stemming from DNA lattice stays constant across GNPs.

In this paper, we discuss and analyze a number of important physical and theoretical aspects that demand a better understanding for quantitative modeling of biosensor response for detection of DNA hybridization and denaturation. The paper is organized as follows. We start with the linear PB model and consider the effects of DNA length, DNA charge distribution, and DNA charge compensation fraction on the sensor response. A self-consistent Donnan equilibrium is also considered to estimate the screening properties inside dense DNA lattices. Then, we present some outcomes of the nonlinear PB theory that predicts much smaller potential variations on the sensor surface upon hybridization. We use the Grahame equation and the standard analytical solutions as well as the numerical analysis to unravel the potential variations on the sensor surface. Finally, we analyze our results and discuss the experimental observations.

2. Basic Equations and Main Results

2.1. Linear PB theory

2.1.1. Analytics for a single-sheet model

For a capacitive EISOI sensor in the constant capacitance mode [35] the potential drop across the gate insulator is constant. Therefore, the changes in the flat-band potential are equal to potential changes at the gate-electrolyte interface [44]. The sensor response is thus the difference in the ES potential at the sensor surface after (φ_{ds}) and before (φ_{ss}) DNA hybridization,

EQ. 3 $$\Delta\varphi = \varphi_{ds}(x=0) - \varphi_{ss}(x=0)$$

For simplicity, as the first step, we project all the DNA charges onto an imaginary plane in the middle of immobilized DNAs at x=L/2 and distribute the charge uniformly with the surface charge density σ. This is the so-called “planar sheet” model of DNA brush first proposed in Ref. [44]. The potential distribution is computed within the linear PB model both in region 1 between the sensor and charged plane ($0 \le x \le L/2$) and in outer electrolyte (region 2, $x \ge L/2$). The general solution of the linear PB equation

EQ. 4 $$\frac{d^2\Psi(x)}{dx^2} = \kappa^2\Psi(x)$$

can be written in regions 1 and 2 in terms of exponential functions [62]

EQ. 5 $$\Psi_1(x) = \alpha e^{\kappa_1 x} + \beta e^{-\kappa_1 x} \quad \text{and} \quad \Psi_2(x) = \gamma e^{-\kappa_2 (x-L/2)}.$$

Here the reciprocal screening lengths are expressed via the [salt] in the corresponding domains

EQ. 6 $$\kappa_{(1,2)} = \sqrt{8\pi l_B n_{0(1,2)}}.$$

The integration constants α, β, γ in EQ. 5 are defined from the boundary conditions. These are given by the Gauss law that relates the derivative of the potential to the charge density on the sensor surface (σ_s) and on DNA sheet (σ). The third condition reflects the potential continuity across the charged plane,

EQ. 7 $$\left(\frac{d\varphi_1}{dx}\right)_{x=0} = -\frac{4\pi\sigma_s}{\varepsilon} > 0,\ \left(\frac{d\varphi_2}{dx}\right)_{x=L/2-0} = -\frac{1}{2}\frac{4\pi\sigma}{\varepsilon} > 0,\ \text{and}\ \ \varphi_1(L/2) = \varphi_2(L/2).$$

The factor ½ in the second equation reflects the fact that only half of the DNA sheet charge influences the potential towards the sensor interface (region 1), while the second half distributes the ions in outer solution (region 2). The integration constants are then given by [44]

EQ. 8 $$\beta = \frac{4\pi l_B}{\kappa_2 e_0}.\frac{\frac{\sigma}{2} + \sigma_s \frac{\kappa_2}{\kappa_1} e^{\kappa_1 L/2}}{2\cosh\left[\kappa_1 L/2\right]},\ \ \alpha = \beta - \frac{4\pi l_B \sigma_s}{\kappa_1 e_0},\ \text{and}\ \ \gamma = \frac{4\pi l_B}{\kappa_2 e_0}\frac{\sigma}{2}.$$

Here, the values for σ_{ss} and σ_{ds} are to be used for σ when computing the potentials from the lattice of ss- and ds-DNAs. Also, the screening length inside the DNA lattice $1/\kappa_1$ can change upon hybridization, so in general $\kappa_1 \neq \kappa_2$, see Sec. 2.1.3. Within the linear PB model, upon DNA hybridization the potential reduction on the sensor surface is independent of its charge density. It is proportional to the differences in charge densities of ds- and ss-DNA sheets, namely

EQ. 9 $$\Delta\varphi = \frac{2\pi(\sigma_{ds} - \sigma_{ss})}{\varepsilon\kappa_2 \cosh\left[\kappa_1 L/2\right]}.$$

In Ref. [44] and in estimates below, we assumed a 100% DNA hybridization efficiency and the same charge fraction for the ss- and ds-DNA, $\theta_{ss}=\theta_{ds}=0.75$. This results in a twice as high potential on ds-DNA charged plane, as compared to ss-DNA "sheet". Counterion condensation significantly reduces the hybridization signals predicted by the linear PB model, but for the situation of $\theta_{ss}\neq\theta_{ds}$ the effects are more subtle, see below. Smaller hybridization efficiencies will of course reduce the contribution from the charged lattice of ds-DNAs.

The charge density of ss-and ds-DNA sheets can be recalculated from the GNP density, ρ_{NGP}, the number of base pairs in immobilized DNAs, $n_{bp} = L/(2l_0)$, and the number of DNA strands adsorbed per GNP, *m*, as follows

EQ. 10 $$\sigma_{ss} = e_0 n_{bp}(1-\theta_{ss}) m \rho_{GNP},\ \sigma_{ds} = 2e_0 n_{bp}(1-\theta_{ds}) m \rho_{GNP}$$

In FIG. 2 we show the potential distribution from the linear PB model for three different screening lengths in region 1 (black curves). Different Debye lengths mimic a possible change in salinity inside dense DNA lattices [56], as compared to the outer low-salt solution used in experiments (at [salt] of 0.2 mM that gives λ_{D2}=210 Å). For comparison, the blue curves illustrate the Debye-Hückel potential decay in the absence of a negative sensor surface. As expected, a lower ionic strength inside the DNA lattice the screening of DNA charges is weaker that gives rise to higher hybridization signals, $\Delta\varphi$. At λ_{D1}=50 Å we get a reduction of sensor potential by $\Delta\varphi\approx$116 mV, close to experimentally detected values as we reported previously in Ref. [44]. This can validate our choice of the one-to-one stoichiometry for the deposition density of ss-DNAs on GNPs, namely *m*=1 used for the linear PB model in Ref. [44] and in FIG. 2. Unfortunately, currently we do not have a reliable experimental technique to determine the average number of ss DNA stands deposited per GNP, for the Au nano-particles of varying sizes and for DNA fragments of varying length.

The maximal ds-DNA packing density on GNPs can be estimated based on geometrical and interaction constraints of a minimal DNA-DNA separation of R≈40 Å and area of one hemi-sphere of GNPs physically available for DNA deposition. This gives the maximum of m=3-4.5 DNAs per GNP, for a typical GNP size used in experiments, D=50-60 Å [44]. For denser DNA lattices, with intermolecular distances of R<40 Å, a strong ES DNA-DNA repulsion emerges [63] that should inhibit the DNA immobilization on GNPs. Despite this, much higher DNA-GNP immobilization densities with the DNA-DNA separations of R≈30 Å were recently shown to be possible too [64] (although for larger13 nm GNPs decorated with DNAs). For the GNPs used in Ref. [44] this DNA density would result in m≈8. This might offer another physical mechanism of sensor signal amplification, apart from the trivial increase of the sensor surface coverage by the DNA on GNP-DNA hybrids. Due to a convex shape and high surface-to-volume ratio of GNPs, the steric as well as ES hindrance between the attached DNA strands gets smaller, as compared to DNA deposition at the same density onto the planar sensor surface. This might enable a deposition of denser DNA spherical brushes on GNPs and thereby "boost" DNA electric change near the sensor surface. The theory of signal amplification by GNPs [43] as such is however beyond the scope of the current paper.

In FIG. 3 we illustrate the effect of the DNA length on the value of sensor potential change upon DNA hybridization, as obtained from the single-sheet linear PB model. The important result here is a non-monotonic dependence of $\Delta\varphi$ described physically as follows. For short DNAs deposited, the DNA charge and the ES potential near the sensor surface are small. As DNA length increases but still stays smaller than the Debye length, the potential change $\Delta\varphi$ progressively increases with *L*.

Once the charged DNA sheet plane at $x=L/2$ is separated by more than 1-2 λ_{D1} from the sensor surface, its ES contribution on the sensor surface is strongly screened. The overall charge effect on the sensor interface becomes therefore non-monotonic: there exists therefore an optimal length of the probe DNAs that maximizes the sensor response. This non-monotonicity prevails also for the charge-distributed model and the Donnan-Debye theory presented below.

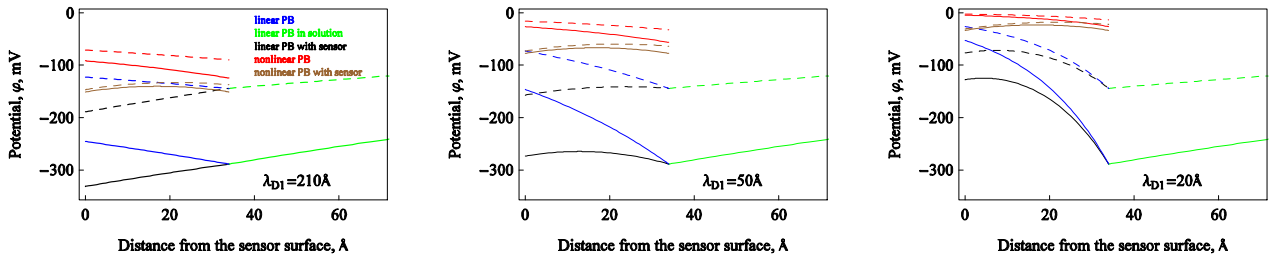

FIG. 2. ES potential profiles between the DNA "plane" and sensor surface before and after DNA hybridization. The solid and dashed curves are respectively for ds- and ss-DNA lattices. The blue and red curves are the potential profiles from the linear and nonlinear PB model for an isolated charge surface at x=L/2. The green and black curves are from the linear PB theory that accounts for a negative sensor surface, EQ. 5. The brown curves are the numerical solutions of nonlinear PB equation with the same boundary conditions, EQ. 7. Parameters: $L/2$=34 Å, DNA length is n_{bp}=20 bp, Debye screening length in the bulk λ_{D2}=210 Å, m=1 (one DNA strand per GNP), DNA charge compensation $\theta_{ss}=\theta_{ds}$=0.75, experimentally observed GNP deposition density $\rho_{GNP}=1.2\times10^{16}$ GNPs/m^2. This choice of parameters gives the charge density of ss-DNA sheet $\sigma_{ss}\approx -e_0/1670$ Å^2, $\sigma_{ds}=2\sigma_{ss}$, and we set the sensor charge density at $\sigma_s=\sigma_{ss}$.

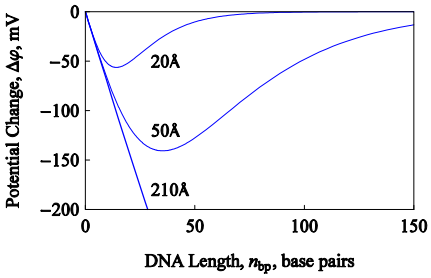

FIG. 3. The change of the sensor surface potential within linear PB model as a function of DNA length. The Debye lengths in DNA lattice denote the corresponding curves; other parameters are the same in FIG. 2.

2.1.2. Distributed DNA charges

The main approximation of a "planar sheet" model above is a "squeezing" all DNA charges onto a uniformly charged plane in the DNA middle. We can relax this assumption, and compute the $\Delta\Psi$ within the linear PB model by summing the exponentially screened ES terms from every bp of immobilized DNAs towards the sensor surface. For this, we divide the adsorbed ss- and ds- 20 bp long DNA lattices into 20 parallel charged "sheets", each with the charge density $\sigma/20$. For every sheet, the linear PB model stays within the limits of its validity, in contrast to the single-sheet-model above.

We obtain that the ES potential is more negative in the DNA middle, at $x=L/2=34$ Å. This is due to stronger overlap of screening ES exponents from both DNA ends. However, the potential difference on the sensor surface at x=0 upon DNA hybridization is quite close to the results of a "single sheet model". The physical reason is that for Debye lengths used $\lambda_{D1}>>L$ and the screened terms from each DNA bp reach the sensor surface with roughly the same magnitude, see left panel in FIG. 4.

On the other hand, when the screening length becomes comparable to the DNA bp separation of 3.4 Å (limit of very high salt), this stratified charge model gives quite different values for $\Delta\Psi$ upon DNA hybridization. In this limit, for the single-sheet model the ES screening "kills" the charge effect from the DNA sheet because $\lambda_{D1}<L/2$. In the multiple-sheet model, the contribution from the sensor-closest DNA bps still survives. In addition, the ES potential along the DNA $\Psi(x)$ unsurprisingly becomes oscillatory, with small maxima at every bp-sheet, with shallow minima in between them, and with overall lower potentials in the DNA middle, see right panel in FIG. 4.

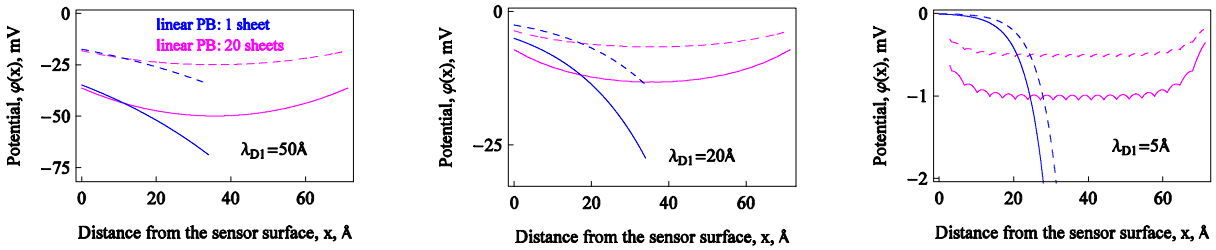

FIG. 4. ES potential for ss-DNA (dashed) and ds-DNA lattices (solid curves) within the model of single (blue) and multiple (magenta) sheets.

2.1.3. Donnan-Debye screening length

Another effect not considered in Ref. [44] is the accumulation of mobile cations attracted from solution into a dense lattice of immobilized DNAs. Within the linear PB theory, the average Donnan potential between DNA fragments ensures the electro-neutrality of DNA lattice. It sets the concentration of mobile cations inside the lattice, which is often much higher than in the bulk solution [57, 53, [65]]. For very dense DNA lattices, like those realized for GNA-GNP deposition, the screening length in solution between DNAs becomes nearly insensitive to bulk [salt], being only the function of DNA lattice density, see FIG. 5. Effectively, the number of positive charges in solution between DNAs should match the number of negative DNA phosphate charges (already partially neutralized by adsorbed cations).

The analytical expression for the Donnan-Debye screening length in the lattice of long cylindrical DNA molecules within the linear PB theory has the form [56]

EQ. 11
$$\lambda_D^{Don} = \lambda_D \left(1 + \left(\frac{4 l_B \lambda_D^2 (1-\theta)}{l_0 \left(R_s^2 - a^2 \right)} \right)^2 \right)^{-1/4} .$$

In application to ss- and ds-DNAs, the corresponding values for the molecular radius *a*, the inter-charge separation along the molecule l_0, and the charge compensation fraction θ are to be taken. The cylindrical cell radius R_s for a DNA lattice is computed from the GNP radius D/2 and number of DNAs *m* immobilized on the upper GNP hemi-sphere, $R_s = \frac{D}{2}\sqrt{\frac{2}{m}}$.

It is easy to show that if the compensation fraction of ds- and ss-DNAs are chosen according to $\theta = 1 - l_0 / l_B$, the Donnan-Debye screening length for ds-DNA lattice is only slightly shorter than for the ss-DNA lattice. The discrepancy is solely due to different molecular diameters for ss- and ds-DNAs. More importantly, in this case the recalculated DNA sheet surface charge densities for ds- and ss-DNA lattice are identical (!) and thus there would be no change in the sensor signal upon DNA hybridization for choise of θs. This contradicts experimental observations and persuades us to use $\theta_{ss}=\theta_{ds}=0.75$, as we did also in [44]. Then, we observe that the Donnan-Debye screening length is measurably shorter for the ds-DNA lattice, as compared to ss-DNA lattice, see FIG. 5. This stronger screening, naturally, reduces the signal from the ds-DNA sheet and attenuates the computed hybridization signal. The latter can be computed via EQ. 9 with $\lambda_{D1} = \lambda_D^{Don}$. These changes in ionic environments inside DNA lattice upon hybridization can be detected by ion-sensitive FEDs, as we proposed in Ref. [57].

As m starts to grow from m=0, the curves for $\Delta\Psi$ with the Donnan equilibrium start to deviate progressively from the results of the linear PB treatment presented above (compare the blue and orange curves in FIG. 5). Then, the potential change reaches a minimum indicating an optimal density of the DNA lattice. Moreover, the sign of the potential change on the sensor surface can change for very dense DNA lattices. Namely, starting from m≈2 the potential change $\Delta\Psi$ becomes positive. The reason is as follows. The ss-DNA sheet which is less screened has a stronger effect on the sensor than twice-

as-charged ds-DNA sheet screened more efficiently because $\lambda_{D,ds}^{Don} < \lambda_{D,ss}^{Don}$. This might indeed be a relevant effect for very dense DNA lattices.

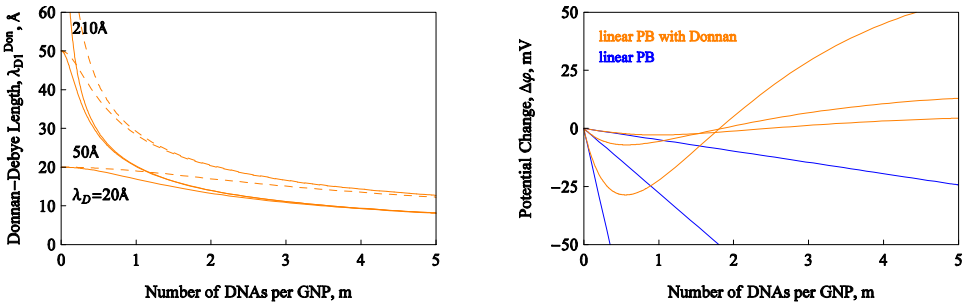

a b

FIG. 5. The Donnan-Debye screening length in GNP-DNA lattice (a) and the potential change on the sensor surface (b), as a function of DNA packing density. Parameters: $a_{ds} = 9$ Å, $a_{ss} = a_{ds}/2$, $\theta_{ds} = \theta_{ss} = 0.75$. Other parameters are the same as in FIG. 2. The values for the Debye length in the bulk denote the corresponding curves.

2.2. Nonlinear PB model

2.2.1. Grahame equation

As we have seen above, particularly in low-salt conditions, the linear PB potentials strongly exceed the applicability limits of the model. So, below we utilize a non-linear PB approach and use the Grahame equation. The latter nonlinearly couples the ES potential of a charged plane φ_0 with its surface charge density σ_0, see Section 12.12 in Ref. [66],

EQ. 12 $$\sinh\left(\frac{\Psi_0}{2}\right) = \frac{2\pi l_B \sigma_0}{\kappa e_0}.$$

The solution of the nonlinear PB equation

EQ. 13 $$\frac{d^2\Psi(x)}{dx^2} = \kappa^2 \sinh[\Psi(x)]$$

for the decay of ES potential from a single planar charged interface at potential Ψ_0 is given by (see EQ. 12.39 in Ref. [66], the potential is given in mV)

EQ. 14 $$\Psi(x) \approx 25.69 \times 2\ln\left[1 + \frac{2\tanh(\Psi_0/4)e^{-\kappa x}}{1 - \tanh(\Psi_0/4)e^{-\kappa x}}\right].$$

For small potentials, when $\Psi_0 << 1$, The Grahame equation reduces to the known linear Ψ-σ relationship for a charged interface, $\varphi_0 = 4\pi\sigma_0/(\varepsilon\kappa)$, and the nonlinear solution turns into the Debye-Hückel limit used in the previous Section, namely

EQ. 15 $$\varphi(x) = \varphi_0 e^{-\kappa x}.$$

Using these non-linear relations, in FIG. 2 we show the potential distributions from the sheets of ds- and ss-DNAs (the solid and dashed curves, respectively). For the weakest screening inside the DNA lattice, for λ_{D1}=210 Å, the potential reduction on the sensor surface due to DNA hybridization is only $\Delta\varphi \approx 20$ mV in the nonlinear model, much smaller than ≈143 mV in the linear case for the same parameters, as reported in Ref. [44]. Overall, for highly charged DNA layers the magnitude of the nonlinear ES potential is considerably smaller than from the linear PB theory (compare red and black curves in FIG. 2). This is the main insight from the nonlinear PB model. This is due to a weak, logarithmic dependence $\Psi_0(\sigma_0)$ in Grahame

equation that describes the saturation in the surface potential Ψ_0 with increase of the interface charge density. This point is illustrated in FIG. 6, where the plane charge density is shown in relevant units (the number of e_0 charges per 1000 Å^2 on the surface). This non-linearity also hampers an accurate theoretical estimation of the density of adsorbed DNAs per GNP based on comparison of the calculated potential differences $\Delta\Psi$ with the experimentally observed values [44].

Also, in the nonlinear PB model for high potentials, $|\Psi|>>1$, the potential decay from the charged surface is faster than the exponential one. Ones the potential decreases down to ~25 mV in a thin nonlinear screening layer near the surface, the exponential screening and the Debye-Hückel model becomes valid again.

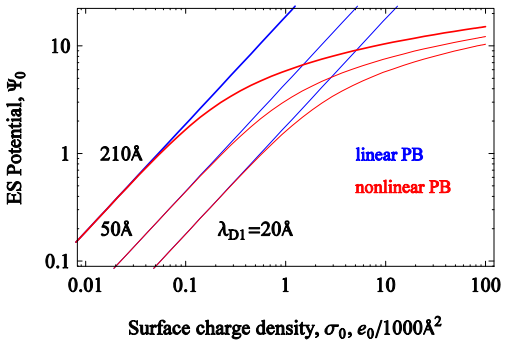

FIG. 6. Dimensionless ES potential versus the surface charge density for linear (EQ. 15, blue curves) and nonlinear (EQ. 14, red curves) PB models. The corresponding bulk Debye lengths are shown near the curves.

2.2.2. Numerical solution

Numerical solution of EQ. 13 in the region between the charged DNA sheet and sensor surface is shown in FIG. 2 as the brown curves. The same boundary conditions as for the linear PB theory were used, see EQ. 7. The results for $\Delta\Psi$ on the sensor surface is even smaller than in simple estimate for a single charge surface (compare the brown and red curves) and of course much smaller than the solution of the linear PB model.

In the nonlinear PB model, the value of $\Delta\Psi$ becomes quite sensitive to the ES potential on the negatively charged sensor surface. This is another physical effect not captured by the linear PB model. Although the DNA hybridization experiments reported in Ref. [44] were performed at pH=7.5 in solution, the concentration of H^+ ions near the sensor surface is not well known experimentally. The charge density and the surface potential of SiO_2 interface however depend strongly on the pH value. The ES potential, for instance, decreases by ≈40 mV per one decade of pH change, starting from the point of zero charge for SiO_2 at pH_{pzc}≈2.2 up to pH=9 [67, 68].

So, we study the dependence of the predicted hybridization signal, $\Delta\Psi = e_0\Delta\varphi/(k_BT)$, upon the sensor charge density σ_s via solving numerically the nonlinear EQ. 13. We observe that the potential change upon DNA hybridization is maximized for relatively weakly charged sensor surfaces, see FIG. 7. For highly charged sensors, to satisfy the ES boundary conditions, the solutions for the potential of ss- and ds-DNA sheet near the sensor surface are very close to one another. This, naturally, yields a smaller sensor response, $\Delta\varphi = \varphi_{ds}(x=0) - \varphi_{ss}(x=0)$, see FIG. 8.

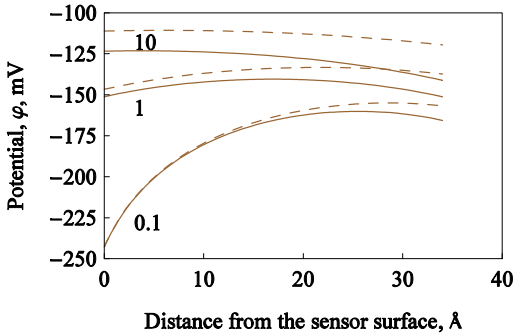

FIG. 7. Variation of ES potential with the sensor surface charge density σ_s in the nonlinear PB model. Dashed and solid curves are for the ss- and ds-DNA sheets. The notations near the curves are related to the surface per unit charge on the sensor surface, as compared to the value used in FIG. 2, i.e., the parameters are $\sigma_s \approx -e_0/(0.1\times 1670\ \text{Å}^2)$, $\sigma_s \approx -e_0/(1\times 1670\ \text{Å}^2)$, and $\sigma_s \approx -e_0/(10\times 1670\ \text{Å}^2)$. Other parameters are the same as in FIG. 2 and λ_{D2}=210 Å.

Numerical solution also reveals that there exists an optimum charge density of the DNA lattice that maximizes the sensor signal $\Delta\Psi$ upon DNA hybridization. This is in drastic contrast to the linear PB model, where the sensor response is just proportional to the number of DNAs immobilized per GNP, m, see Ref. [44] and FIG. 5b above. Weakly charged sensor surfaces yield larger potential differences $\Delta\Psi$. This maximal-response regime occurs at DNA/GNP density of m~0.3-2 that is a physical range of DNA lattice density achievable by modern DNA-GNP deposition techniques. For instance, the value of m=1 was chosen in Ref. [44] and in FIG. 2 above for the linear PB model. Of course, as m$\to$0 the potential difference $\Delta\Psi$ also vanishes. Overall, the sensor signals $\Delta\Psi$ are larger for weaker screening, as expected, see FIG. 8a. For shorter screening lengths inside DNA lattices, at λ_{D1}=20 Å, the density of the DNA sheet that gives the maximal sensor response becomes slightly larger, with m=1-3 DNAs adsorbed per GNP, see FIG. 8c.

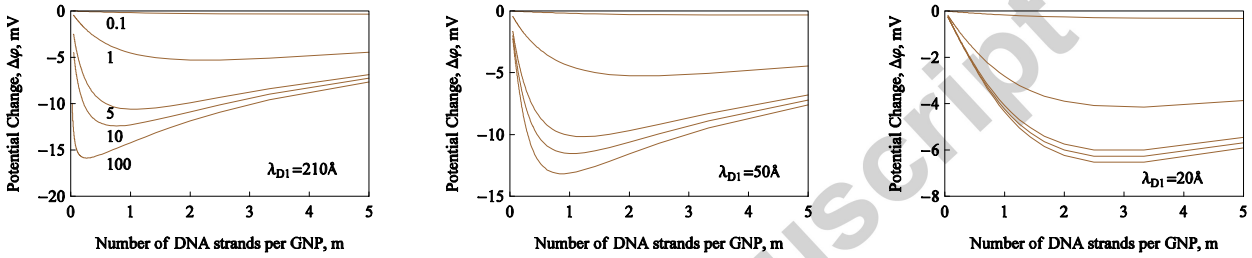

FIG. 8. Variation of the potential change on the sensor surface upon DNA hybridization, $\Delta\varphi$, as a function of DNA lattice charge density. The results are plotted for 5 values of the sensor surface charge density, with the area per charge being $-e_0/\sigma_s$=(0.1, 1, 5, 10, 100)$\times$1670 Å^2 (denoting the curves from top to bottom).

3. Conclusions and Outlook

In this paper, we have studied theoretically the effects of several important physical parameters on the potential changes $\Delta\Psi$ and the response of FED biosensors upon DNA hybridization on their surfaces. In the linear PB model, we presented some analytical results for the ES potential that is a sensitive function of electrolyte concentration (lower solution salinities give higher sensor signals) and the length of immobilized DNA probes. Namely, the values of potential $\Delta\Psi$ computed reveal a non-monotonic dependence with DNA length *L*. This is the 1st new theoretical result. This reflects the interplay of a linear increase of DNA charge with *L* and a much stronger, exponential screening of DNA charges which are farther away from the sensor-electrolyte interface. The model thus describes strongly decreasing sensor signals for DNA half-length *L*/2 that is longer than several λ_D. The application of GNP-DNA hybrids for detection of long DNA fragments, with *L*>50 bp, will also be hindered by DNA steric effects. Namely, because of a pronounced coiling of long ss-DNA chains, an efficient and relatively fast DNA hybridization with complementary target ss-DNAs will no longer be possible. A reduction of the DNA lattice density will help hybridization, but then the overall DNA electric charge and the ES potential will decrease progressively. These factors strongly limit the applicability of the EISOI FED devices for a reliable detection of DNA oligo-nucleotide sequences longer than 50-100 bp from unknown DNA mixtures.

We have also examined the effects of ionic equilibrium via a self-consistent Donnan-Debye screening inside the DNA lattice. For moderately charged DNA lattices, a stronger screening inside the ds-DNA lattice results in a reduced DNA hybridization signal. This is the 2nd important insight from the theory. The implications of DNA charge discreteness have been analyzed as well. For realistic screening lengths and DNA lattice charge density, the linear PB model predicts the hybridization signals $\Delta\varphi \approx$100 mV that is in good agreement with the experiment [44].

We have shown that DNA charge density has a simple effect in the linear PB model but $\Delta\varphi$ exhibits saturation in the nonlinear PB theory. For the latter, both analytically and numerically, we predicted that the sensor response signals are much smaller than the overestimated linear PB values. The signals are also smaller than the experimentally detected $\Delta\varphi$

=90-120 mV upon the probe-target DNA hybridization and melting. This is due to a nonlinear potential saturation with the DNA lattice charge density in this limit: potential variations even for the weakest screening do not exceed $\Delta\varphi$ =20 mV, irrespective how high the DNA deposition density on GNPs will be. This is the 3rd new theoretical result. Some additional factors, on top of the DNA electric charge brought to the sensor surface upon hybridization, might of course somewhat affect the magnitude of theoretical predictions. The inherent ES saturation effects in the nonlinear PB model however severely limit its applicability for the description of about 100 mV potential signals measured experimentally upon DNA hybridization. This challenges future theoretical studies in this direction.

Of course, our outcomes regarding the screening of electric charges near a biosensor surface as well as the ionic equilibrium are equally applicable to the description of adsorption of other charged analytes on the biosensor surface, such as proteins, enzymes, polyelectrolytes, viruses, and bacteria [69, 70, 71, 72].

As an outlook, we touch on several aspects of sensor functioning which still remain to be understood better, both experimentally and theoretically. One of them is the recognition of only partially matched ss-DNA sequences (DNA nucleotide polymorphism), in contrast to fully-matched and fully-mismatched target ss-DNA as implemented in Ref. [44]. For instance, how the hybridization efficiency will depend on the position of a single nucleotide mismatch along the probe DNA [73] and how long can the DNA sequence be to still sense this bp-mismatch? How can one model this partial DNA non-commensuration via a DNA hybridization efficiency parameter (that we put unity in the model above)? Second, the sensitivity of GNP-DNA FED sensors has to be determined more precisely, down to at least nM target DNA concentrations, as compared to relatively high 5 μM of target ss-DNA used in experiments so far [44,45]. The work in this direction is in progress.

Last but not least, it would be of great advantage for various detection purposes to know the selectivity of GNP-DNA FED sensors [44], particularly for situations when differently mismatched ss-DNA sequences are present in abundance in DNA mixtures. What is the efficiency of detecting a fully-matched target ss-DNA under such conditions and how does it compare to the detection sensitivity of a standard biochip-based technique? This poses a number challenges for future experimental developments of FED DNA biosensors with a desired level of sensitivity and specificity, working in a broad range of system parameters (such DNA length, target-DNA concentration, nucleotide mismatch position, and solution salinity).

4. Acknowledgements

I acknowledge the support by the Deutsche Forschungsgemeinschaft (DFG Grant CH 707/5-1) and scientific discussions with A. Poghossian and M. Weil.

[1] J.-P. Knemeyer et al., Anal. Chem., 72 3717 (2000).
[2] C. Y. Zhang et al., Nature Mater., 4 826 (2005).
[3] G. Braun et al., J. Am. Chem. Soc., 129 6378 (2007).
[4] G. H. Wu et al., PNAS, 98 1560 (2001).
[5] J. Fritz et al., PNAS, 99 14142 (2002).
[6] P. S. Waggoner and H. G. Craighead, Lab on a Chip, 7 1238 (2007).
[7] J. Fritz, Analyst, 132 855 (2008).
[8] T. Endo et al., Analyt. Chemistry, 77 6976 (2005).
[9] M. L. Diakité et al., Lab on a Chip, 12 4738 (2012).
[10] E. Stern et al., Nature, 445 519 (2007).
[11] Z. Li et al., Nano Lett., 4 245 (2004).
[12] S. Sorgenfrei et al., Nature Nanotech., 6 126 (2011).
[13] F. W. Scheller et al., Curr. Opin. Biotechnol., 12 35 (2001).
[14] M. J. Schöning and A. Poghossian, Analyst, 127 1137 (2002).
[15] J. S. Daniels and N. Pourmand, Electroanalysis, 19 1239 (2007).
[16] G. Gruner, Analyt. Bioanalyt. Chem., 384 322 (2006).
[17] T. W. Lin et al., Biosens. Bioelectron., 25 2706 (2010).
[18] C. E. Nebel et al., J. Phys. D: Appl. Phys., 40 6443 (2007).
[19] H. X. Li and L. J. Rothberg, J. Am. Chem. Soc., 126 10958 (2004).
[20] C. S. J. Hou et al., Lab on a Chip, 7 347 (2007).
[21] G. M. Credo et al., Analyst, 137 1351 (2012).
[22] J. L. Abell et al., J. Am. Chem. Soc., 134 12889 (2012).
[23] X. Tang et al., Nano Lett., 6 1632 (2006).
[24] K. Maehashi et al., Analyt. Chemistry, 79 782 (2007).
[25] M. T. Martinez et al., Nano Lett., 9 530 (2009).
[26] A. Merkoci et al., Trends Analyt. Chem., 24 826 (2005).

[27] A. Merkoci, Microchim. Acta, 152 157 (2006).
[28] M. Kwiat et al., J. Am. Chem. Soc., 134 280 (2012).
[29] A. Sassolas et al., Chem. Rev., 108 109 (2008).
[30] A. Revzin et al., Biomicrofluidics, 6 021301 (2012).
[31] W. A. Lai et al., Biosens. Bioelectron., 35 456 (2012).
[32] K. H. Lee et al., Biosens. Bioelectron., 31 343 (2012).
[33] B. van Grinsven et al., ACS Nano, 6 2712 (2012).
[34] T. Goda and Y. Miyahara, Biosens. Bioelectron., 32 244 (2012).
[35] A. Poghossian et al., Biosens. Bioelectron., 22 2100 (2007).
[36] B. K. Wunderlich, P. A. Neff, and A. R. Bausch, Appl. Phys. Lett., 91 083904 (2007).
[37] I. Y. Wong and N. A. Melosh, Biophys. J., 98 2954 (2010).
[38] J. W. Zwannikken et al., J. Phys. Chem C, 115 16368 (2011).
[39] A. Bulyha and C. Heitzinger, Nanoscale, 3 1608 (2011).
[40] M. W. Shinwari and M. J. Deen, J. Electrochem. Soc., 158 J189 (2011).
[41] M. T. Castaneda et al., Electroanalysis, 19 743 (2007).
[42] K. Saha et al., Chem. Rev., 112 2739 (2012).
[43] X. Cao et al., Analyt. Biochem., 417 1 (2011).
[44] M. H. Abouzar et al., Phys. Status Solidi A, 209 925 (2012).
[45] M. H. Abouzar, PhD Thesis, HU Berlin, (2011).
[46] M. H. Abouzar et al., Biosens. Bioelectron., 26 3023 (2011).
[47] A. Poghossian et al., Biosens. Bioelectron. 22 2100 (2007).
[48] A. Poghossian et al., Appl. Phys. A, 87 517 (2007).
[49] M. H. Abouzar et al., Phys. Stat. Solidi A, 207 884 (2010).
[50] Y. Zhang et al., Intl. J. Electrochem., (2012) doi:10.4061/2012/619782
[51] G. S. Manning, Quart. Rev. Biophys., 11 179 (1978).
[52] G. S. Manning, Macromolecules, 34 4650 (2001).
[53] A. G. Cherstvy, Phys. Chem. Chem. Phys., 13 9942 (2011).
[54] A. G. Cherstvy, J. Phys. Chem. B, 114 5241 (2010).
[55] D. B. McIntosh and O. A. Saleh, Macromolecules, 44 2328 (2011).
[56] A. G. Cherstvy and A. A. Kornyshev, J. Phys. Chem. B, 109 13024 (2005).
[57] A. Poghossian et al., Sens. & Actuators B, 111-112 470 (2005).
[58] A. G. Cherstvy and R. G. Winkler, Phys. Chem. Chem. Phys., 13 11686 (2011).
[59] G. Lamm, Reviews Comput. Chem., 19 147 (2003).
[60] A. G. Cherstvy, J. Phys. Chem. B, 111 7914 (2007).
[61] I. Y. Wong and N. A. Melosh, Nano Lett., 9 3521 (2009).
[62] A. G. Cherstvy and R. Everaers, J. Phys.: Cond. Mat., 18 11429 (2006).
[63] A. G. Cherstvy, J. Mol. Recognit., 24 283 (2011).
[64] A. E. Prigodich et al., J. Am. Chem. Soc., 132 10638 (2010).
[65] J. Schultz et al., Biophys. J., 66 810 (1994).
[66] J. Israelachvili, "Intermolecular and surface forces", Academic Press, (1992).

[67] P. Bergveld, A. Sibbald, Analytical and biomedical applications of ion-selective-field-effect-transistors, ed. G. Svehla, Analytical Chemistry, Vol. XXIII, Elsevier, (1988).
[68] R. E. G. van Hal, J. C. T. Eijkel, P. Bergveld, Adv. Colloid Interface Sci., 69 31 (1996).
[69] A. B. Kayitmzer et al., Soft Matter, (2013), DOI: 10 .1039/c2sm27002a
[70] A. Poghossian et al., Analyt. Bioanalyt. Chem, submitted (2013).
[71] E. Wischerhoff et al., Soft Matter, 6 705 (2010).
[72] G. Shalev et al., Biosens. Bioelectron., 31 510 (2012).
[73] N. E. Marotta et al., Analyt. Chem., 85 1440 (2013).

- Electrostatic model of signal generation for DNA biosensors with Au nano-particles is developed
- Influence of separation of charged analytes form the sensor surface is studied
- Linear and nonlinear Poisson-Boltzmann models are used; Donnan effect in dense DNA brushes
- Nonlinear model predicts much weaker sensor response upon DNA hybridization
- Charge neutralization, length and spatial conformations of deposited DNAs are analyzed